Spectral-Efficient Gapped Index Modulation for FTN-mCAP in Bandlimited VLC

Yungui Nie, Chen Chen, Senior Member, IEEE, Zhihong Zeng, Xiaodi You, Harald Haas, Fellow, IEEE, and Gangxiang Shen, Senior Member, IEEE, Fellow, Optica

Abstract—A low-complexity gapped index modulation (GIM) scheme was proposed to mitigate inter-band interference (IBI) in faster-than-Nyquist multi-band carrierless amplitude and phase modulation (FTN-mCAP), but incurs spectral efficiency (SE) loss due to silent subbands. To address this, three spectral-efficient GIM schemes are proposed. First, the quadrature GIM aided FTN-mCAP (FTN-mCAP-QGIM) is proposed, and an enhanced LLR detector is designed accordingly. Second, a variable GIM aided FTN-mCAP (FTN-mCAP-VGIM) scheme is proposed to support variable subband activation. Third, a variable quadrature GIM aided FTN-mCAP (FTN-mCAP-VQGIM) is proposed to further enhance the SE of FTN-mCAP-VGIM. Extensive simulations and hardware experiments are conducted to evaluate the performance of three spectral-efficient GIM schemes. The experimental results demonstrate that FTN-8CAP-VQGIM supports a compression factor of 0.53 at a target bit error rate (BER) of  $3.8 \times 10^{-3}$ , and achieves a 113% enhancement in SE compared with 8CAP.

Index Terms—Visible light communication, carrierless amplitude and phase modulation, faster-than-Nyquist.

# I. INTRODUCTION

ITH the continuous advancement of sixth-generation (6G) communication technologies, the data transmission demands in frontier fields, such as artificial intelligence (AI), are expected to experience exponential growth. However, the scarcity of spectrum resources limits the enhancement of radio frequency (RF) communication capacity [1]. Visible light communication (VLC), with several advantages such as abundant spectrum resources, high security and low cost, can serve as a viable alternative to RF communication [2], [3]. However, the data rate of light emitting diode (LED)-based VLC systems is constrained by the limited modulation bandwidth of the LED, typically in the few-MHz range [4].

To extend the available modulation bandwidth of the VLC system, pre-equalization [5] and post-equalization [6] have

This work was supported by the National Natural Science Foundation of China under Grants 62271091 and 62001319, the Suzhou Science and Technology Bureau-Technical Innovation Project in Key Industries under Grant SYG202112, and the Open Fund of IPOC (BUPT) under Grant IPOC2020A009. (Corresponding authors: Chen Chen; Gangxiang Shen)

Y. Nie, X. You, and G. Shen are with the Jiangsu New Optical Fiber Technology and Communication Network Engineering Research Center, Suzhou Key Laboratory of Advanced Optical Communication Network Technology, Institute for Broadband Research & Innovation (IBRI) and School of Electronic and Information Engineering, Soochow University, Suzhou, Jiangsu 215006, China (e-mail: shengx@suda.edu.cn).

C. Chen, and Z. Zeng are with the School of Microelectronics and Communication Engineering, Chongqing University, Chongqing 400044, China (e-mail: c.chen@cqu.edu.cn).

Harald Haas is with the Department of Engineering, University of Cambridge, CB2 1PZ Cambridge, U.K.

been widely used. On the other hand, when the modulation bandwidth of the LED is fixed, spectrally efficient schemes such as carrierless amplitude and phase modulation (CAP) [7] and orthogonal frequency division multiplexing (OFDM) [8] have been proven effective in improving the data rate of VLC systems. Compared to OFDM, CAP offers the advantages of lower peak-to-average power ratio (PAPR) and reduced implementation complexity. As the demand for higher data rate and better adaptability to complex environments grows, research into multi-band CAP (mCAP) has emerged as a key focus [9]. In order to achieve higher spectral efficiency (SE), fasterthan-Nyquist mCAP (FTN-mCAP) [10], [11], [12], regarded as an enhanced version of mCAP, has proposed. However, as spectrum compression increases, FTN sampling causes more severe inter-band interference (IBI). Several IBI mitigation schemes have been studied for FTN-mCAP. Most of them suffer from high complexity, relying on techniques such as LMS-Volterra filtering [10], machine learning [13], neural networks [11] and Tomlinson-Harashima precoding (THP) [12]. Recently, a new gapped index modulation (GIM) [14] has been implemented on the transmitter side to mitigate the IBI, which transmits signals by activating k gapped subbands out of m, leaving the silent subbands to eliminate IBI. However, the silent subbands in GIM scheme leads to a non-negligible

To further improve the SE of bandlimited VLC systems, we propose three spectral-efficient GIM schemes: quadrature GIM aided FTN-mCAP (FTN-mCAP-QGIM), variable GIM aided FTN-mCAP (FTN-mCAP-VGIM) and variable quadrature GIM aided FTN-mCAP (FTN-mCAP-VQGIM). The main contributions of this work are as follows: three spectral-efficient GIM schemes are first proposed to further improve the SE and an enhanced LLR detector is designed for FTN-mCAP-QGIM. The superiority of the proposed scheme is validated by extensive simulations and experimental results.

# II. PRINCIPLE

## A. Principle of FTN-mCAP-QGIM

Figs. 1(a) and (b) illustrate the principles of FTN-mCAP-QGIM transmitter and receiver, respectively. In the FTN-mCAP-QGIM mapper, the input b bits are fed into the bit splitter, dividing the total b bits into three parts:  $b_{\rm C}$ ,  $b_{\rm I}$  and  $b_{\rm Q}$ . In the meantime, the total of m subbands are categorized into activated and silent states. More specifically, the first part  $b_{\rm C}$  bits are mapped to M-ary quadrature amplitude modulation (M-QAM) symbols on the k activated subbands, whose inphase and quadrature components are then separated by an

1

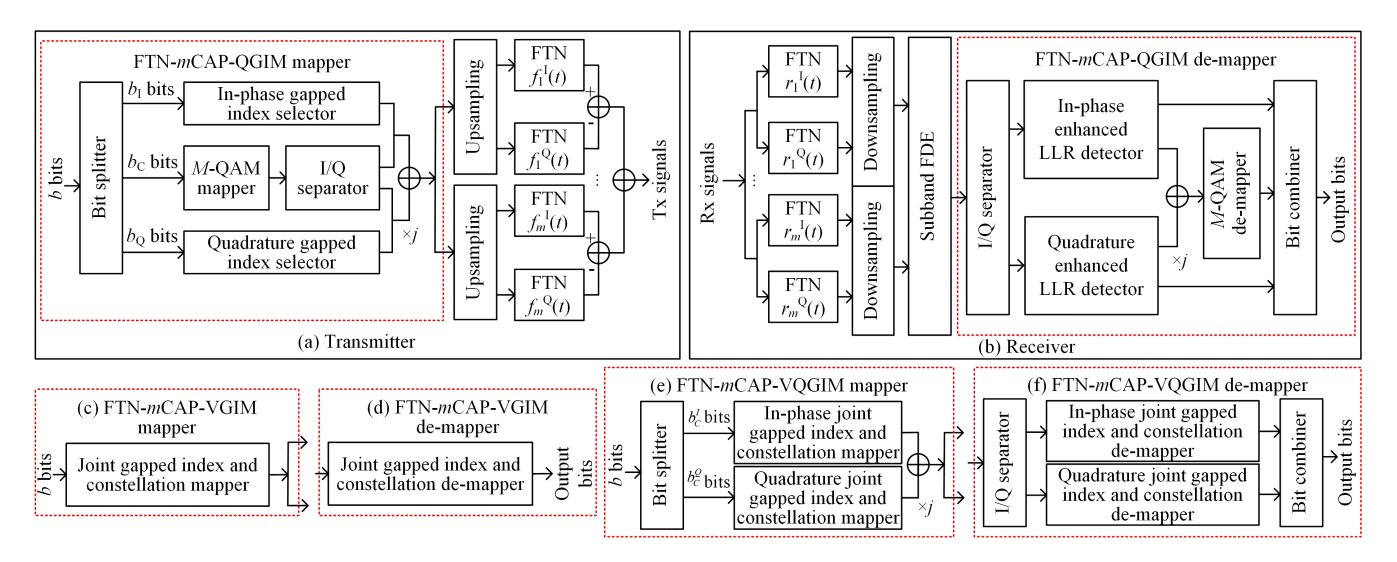


Fig. 1. Principles of (a) the transmitter and (b) the receiver of FTN-mCAP-QGIM; (c) the mapper and (d) the de-mapper of FTN-mCAP-VGIM; and (e) the mapper and (f) the de-mapper of FTN-mCAP-VQGIM.

I/Q separator. The remaining  $b_{\rm I}$  and  $b_{\rm Q}$  bits are respectively used to determine the in-phase and quadrature gapped indexes of k activated subbands out of m. The gapped indexes of FTN-6CAP-QGIM with k = 3 corresponding to in-phase component contain {1, 3, 5}, {1, 3, 6}, {1, 4, 6}, {2, 4, 6}. The example of FTN-8CAP-QGIM with k = 4 mapping table is illustrated in Table I, where  $\bar{I} = \{\bar{I}^{I}, \bar{I}^{Q}\}$  is the gapped index set. Additionally, the gapped indexes of FTN-6CAP-QGIM with k = 2 corresponding to in-phase component contain  $\{1, 3\}$ ,  $\{1, 4\}, \{1, 5\}, \{1, 6\}, \{2, 4\}, \{2, 5\}, \{2, 6\} \text{ and } \{3, 6\},$ and the gapped indexes of FTN-8CAP-QGIM with k = 2corresponding to in-phase component contain {1, 3}, {1, 4},  $\{1, 5\}, \{1, 6\}, \{1, 7\}, \{1, 8\}, \{2, 5\}, \{2, 6\}, \{2, 7\}, \{2, 6\}, \{2, 7\}, \{2,$ 8},  $\{3, 6\}$ ,  $\{3, 7\}$ ,  $\{3, 8\}$ ,  $\{4, 7\}$ ,  $\{4, 8\}$  and  $\{5, 8\}$ . The inphase and quadrature components share the same gapped index set. Hence, the SE for FTN-mCAP-QGIM with M-QAM constellation in bandlimited VLC systems can be expressed as follows

$$SE_{\text{FTN-}m\text{CAP-QGIM}} = \frac{b_{\text{I}} + b_{\text{Q}} + k \log_2(M)}{(1 + \alpha)(1 - \beta)m}, \tag{1}$$

where  $\alpha$  and  $\beta$  ( $0 \le \beta \le 1$ ) denote the roll-off factor of the square-root raised cosine (SRRC) filter and the spectrum compression factor, respectively, with  $\alpha$  set to 0.5. B is the total bandwidth before spectrum compression. The remaining steps are detailed in [14].

In the FTN-mCAP-QGIM de-mapper, to reduce the detection errors of log-likelihood ratio (LLR) detector, the enhanced LLR detection is performed separately on the in-phase and quadrature components. The index combinations used in FTN-mCAP-QGIM scheme are regarded as legal gap indexes, and those not used are illegal. Here, we focus on the detection of the in-phase component as an example. For the enhanced LLR detection, LLR detection is first performed, followed by a comparison of the detected gapped indexes with the gapped indexes used at the transmitter side. If an unused gapped index is found, it is considered a detection error and recorded as an illegal gapped index. The signal is extracted and the ML

TABLE I THE EXAMPLE OF FTN-mCAP-QGIM WITH m = 8 and k = 4 mapping table.

Index bits	$\{\bar{I}^{\mathrm{I}},\bar{I}^{\mathrm{Q}}\}$	Index bits	$\{ar{I}^{\mathrm{I}},ar{I}^{\mathrm{Q}}\}$
0 0 0 0	{1, 3, 5, 7, 1, 3, 5, 7}	1000	{1, 4, 6, 8, 1, 3, 5, 7}
0 0 0 1	{1, 3, 5, 7, 1, 3, 5, 8}	1001	{1, 4, 6, 8, 1, 3, 5, 8}
0 0 1 0	{1, 3, 5, 7, 1, 4, 6, 8}	1010	{1, 4, 6, 8, 1, 4, 6, 8}
0 0 1 1	{1, 3, 5, 7, 2, 4, 6, 8}	1 0 1 1	{1, 4, 6, 8, 2, 4, 6, 8}
0 1 0 0	{1, 3, 5, 8, 1, 3, 5, 7}	1 1 0 0	{2, 4, 6, 8, 1, 3, 5, 7}
0 1 0 1	{1, 3, 5, 8, 1, 3, 5, 8}	1 1 0 1	{2, 4, 6, 8, 1, 3, 5, 8}
0 1 1 0	{1, 3, 5, 8, 1, 4, 5, 8}	1 1 1 0	{2, 4, 6, 8, 1, 4, 6, 8}
0 1 1 1	{1, 3, 5, 8, 2, 4, 6, 8}	1111	{2, 4, 6, 8, 2, 4, 6, 8}

detection is performed separately. Considering the 7% forward error correction (FEC) coding limit, LLR detection achieves a relatively low detection error probability, while the proposed enhanced LLR further improves the detection accuracy of LLR detection. Compared with LLR, the additional complexity of enhanced LLR lies in performing ML detection when a detection error occurs, which is specifically determined by the probability of the occurrence of illegal gapped index.

## B. Principle of FTN-mCAP-VGIM/VQGIM

Figs. 1(c) and (d) illustrate the principles of FTN-mCAP-VGIM mapper and de-mapper, respectively. For the FTN-mCAP-VGIM mapper, the m subbands are treated as a subblock, within which k subbands are activated, with k being variable. The subblock signals are determined by the gapped indexes of the k activated subbands and M-QAM constellation symbols. Let  $\mathcal{K} = \left\{0,1,\ldots,\left\lceil\frac{m}{2}\right\rceil\right\}$  denote the set of activated subbands, where  $\lceil \cdot \rceil$  denotes the ceil operator and  $\left\lceil\frac{m}{2}\right\rceil$  represents the maximum number of subbands that can be activated. Taking m=6 and 8 for example, the gapped indexes of FTN-6CAP-VGIM with  $\mathcal{K} = \left\{0,1,2,3\right\}$  contain  $\left\{0\right\}$ ,  $\left\{1\right\}$ ,  $\left\{3\right\}$ ,  $\left\{4\right\}$ ,  $\left\{6\right\}$ ,  $\left\{1,4\right\}$ ,  $\left\{1,6\right\}$ ,  $\left\{1,3,6\right\}$  and  $\left\{1,4,6\right\}$ , and the gapped indexes of FTN-8CAP-VGIM with  $\mathcal{K} = \left\{0,1,2,3,4\right\}$  contain  $\left\{0\right\}$ ,  $\left\{1\right\}$ ,  $\left\{3\right\}$ ,  $\left\{5\right\}$ ,  $\left\{8\right\}$ ,  $\left\{1,3\right\}$ ,  $\left\{1,5\right\}$ ,  $\left\{1,8\right\}$ ,  $\left\{3,8\right\}$ ,  $\left\{1,3,8\right\}$ ,  $\left\{1,5,8\right\}$ ,  $\left\{2,5,8\right\}$ ,  $\left\{3,5,5\right\}$ 

TABLE II REQUIRED M-QAM CONSTELLATIONS FOR DIFFERENT SCHEMES BASED ON FTN-6CAP AND FTN-8CAP.

Schemes	R = 27.78  Mbps	Schemes	R = 25  Mbps
FTN-6CAP	4/4/4/4/2/2-	FTN-8CAP	4/4/4/4/2/2/2/2-
	QAM		QAM
FTN-6CAP-GIM,	16/8-QAM	FTN-8CAP-GIM,	16-QAM
k = 2	10/6-QAM	k = 2	
FTN-6CAP-GIM,	8/8/4-QAM	FTN-8CAP-GIM,	8/8/4/4-QAM
k = 3	0/0/4-QAIVI	k = 4	
FTN-6CAP-VGIM	8-QAM	FTN-8CAP-VGIM	8-QAM
FTN-6CAP-QGIM,	4-QAM	FTN-8CAP-QGIM,	4-QAM
k = 2	4-QAM	k = 2	
FTN-6CAP-QGIM,	4-QAM	FTN-8CAP-QGIM,	4-QAM
k = 3	4-QAM	k = 4	
FTN-6CAP-VQGIM	4-QAM	FTN-8CAP-VQGIM	4-QAM

8} and  $\{1, 3, 5, 8\}$ . Hence, the SE for FTN-mCAP-VGIM with M-QAM constellation in bandlimited VLC systems can be expressed by

$$SE_{\text{FTN-}m\text{CAP-VGIM}} = \frac{\left[\log_2\left(\sum_{i=0}^{\left\lceil\frac{m}{2}\right\rceil} n_i M^{k_i}\right)\right]}{(1+\alpha)(1-\beta)m}, \quad (2)$$

where  $n_i$  is the number of gapped indexes used when activating  $k_i$  subbands and  $\lfloor \cdot \rfloor$  is the floor operator.

Subsequently, Figs. 1(e) and (f) illustrate the principles of FTN-mCAP-VQGIM mapper and de-mapper, respectively. For the FTN-mCAP-VQGIM mapper, the input b bits are divided into  $b_C^1$  and  $b_C^0$ , each independently mapped using the FTN-mCAP-VGIM mapping process. Hence, the SE for FTN-mCAP-VQGIM in bandlimited VLC systems can be expressed by

 $SE_{\mathrm{FTN-}m\mathrm{CAP-VQGIM}} =$ 

$$\frac{\left\lfloor \log_2 \left( \sum_{i=0}^{\left\lceil \frac{m}{2} \right\rceil} n_i^{\mathrm{I}} \left( M^{\mathrm{I}} \right)^{k_i} \right) \right\rfloor + \left\lfloor \log_2 \left( \sum_{i=0}^{\left\lceil \frac{m}{2} \right\rceil} n_i^{\mathrm{Q}} \left( M^{\mathrm{Q}} \right)^{k_i} \right) \right\rfloor}{(1+\alpha)(1-\beta)m}$$
(3)

where  $n_i^{\rm I}$  and  $n_i^{\rm Q}$  denote the number of gapped indexes used for activating  $k_i$  subbands in the in-phase and quadrature components, respectively. For the FTN-mCAP-VGIM/VQGIM demapper, ML detector is employed for signal detection. The complexity in terms of complex multiplications for FTN-mCAP-VGIM is  $O(2^{SE_{\rm FTN-}m{\rm CAP-VGIM}}m)$ . Similarly, the complexity in terms of complex multiplications for FTN-mCAP-VQGIM is  $O(2^{SE_{\rm FTN-}m{\rm CAP-VQGIM}}m)$ .

#### III. RESULTS AND DISCUSSIONS

In this section, we conduct simulations and experiments to evaluate the performance of three spectral-efficient GIM schemes. The numbers of subbands are set to m=6 and 8, respectively. B is fixed at 25 MHz. To ensure a fair comparison at the same data rate R, the required M-QAM constellations for different schemes are summarized in Table II.

First, as shown in Fig. 2(a), we analyze the performance of different detectors for FTN-6CAP-QGIM over the AWGN channel. We can observe that the enhanced LLR detector achieves better BER performance than LLR detector, and

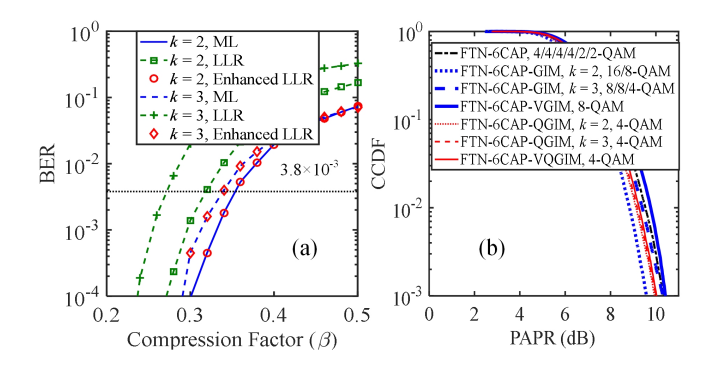


Fig. 2. (a) Comparison of different detectors for FTN-6CAP-QGIM, and (b) PAPR comparison for different schemes based on FTN-6CAP.

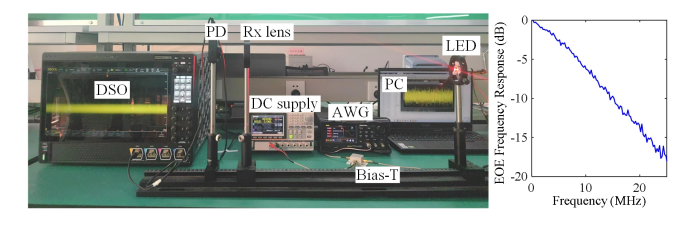


Fig. 3. Experimental setup of the VLC system based on red LED. Inset: frequency response of the complete experimental system.

nearly the same BER performance as the ML detector. Fig. 2(b) compares the PAPR performance of different schemes based on FTN-6CAP with  $\beta$  = 0.3. It can be observed that the different schemes based on FTN-6CAP all achieve PAPR values of approximately 10 dB at the probability of  $1 \times 10^{-3}$ .

Subsequently, the experimental setup of a point-to-point VLC system is illustrated in Fig. 3. The sampling rates of arbitrary waveform generator (AWG, Rigol DG2102) and digital storage oscilloscope (DSO, Rigol DS70504) are 60 and 500 MSa/s, respectively. The inset in Fig. 3 depicts the measured frequency response of the system. We can see that the system exhibits a distinct low-pass characteristic, with the measured -3 dB bandwidth of about 6 MHz.

Fig. 4 presents the experimental BER versus compression factor for different schemes based on FTN-mCAP, where the peak-to-peak voltage (Vpp) is set to 6.8 V. We can observe that as the spectrum compression increases, the BER performance gradually deteriorates, primarily due to the increased IBI. For the case of m = 6, as shown in Fig. 4(a), FTN-6CAP-GIM with k = 3 achieves the largest compression factor of 0.34 to reach the 7% FEC coding limit of BER =  $3.8 \times 10^{-3}$ , compared with FTN-6CAP, FTN-6CAP-GIM with k = 2 and FTN-6CAP-VGIM. After introducing quadrature GIM, FTN-6CAP-VQGIM achieves the largest compression factor of 0.41 among all the schemes. For a relatively high value of m = 8, it can be observed that, under the 7% FEC coding limit of BER =  $3.8 \times 10^{-3}$ , except for the FTN-8CAP-GIM with k = 2 scheme, the remaining schemes based on FTN-8CAP-GIM achieve greater spectrum compression than FTN-8CAP. Importantly, FTN-8CAP-VQGIM supports the largest spectrum compression of 0.53 compared with the other schemes considered. An SE increases from 1 bit/s/Hz for 8CAP to 2.13 bits/s/Hz for FTN-8CAP-VQGIM, resulting in a substantial SE

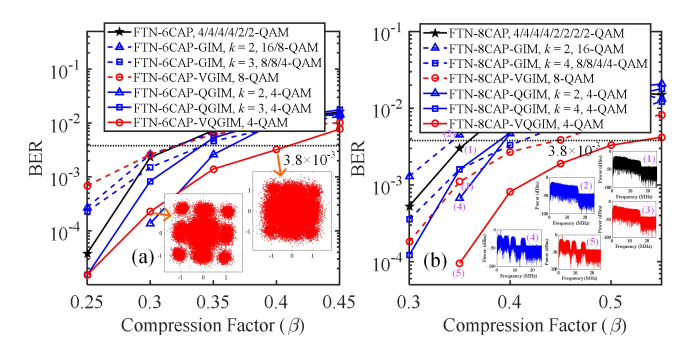


Fig. 4. Experimental BER vs. compression factor for different schemes based on (a) FTN-6CAP and (b) FTN-8CAP.

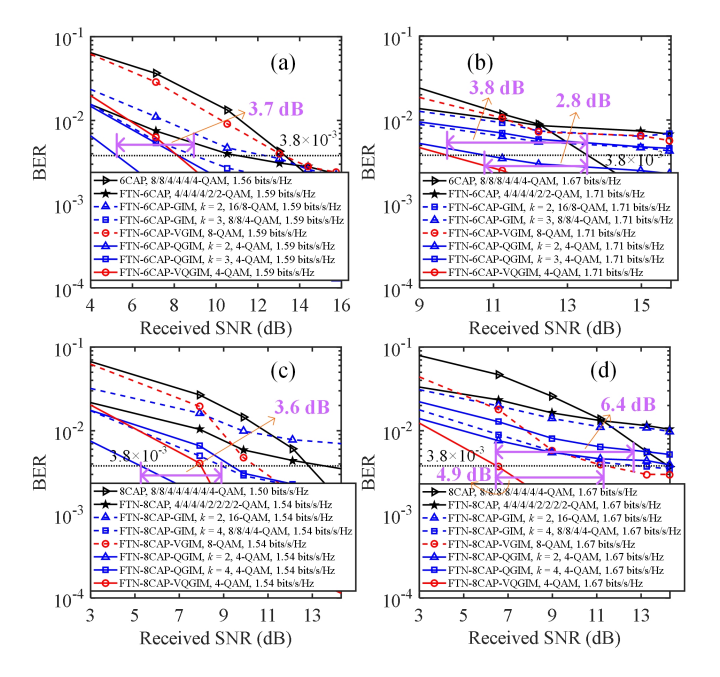


Fig. 5. Experimental BER vs. SNR for different schemes based on FTN-mCAP with (a)  $m=6,\ \beta=0.3$  and (b)  $m=6,\ \beta=0.35,$  (c)  $m=8,\ \beta=0.35$  and (d)  $m=8,\ \beta=0.4.$ 

enhancement of 113%. The insets in Figs. 4(a) and (b) depict the received constellation diagrams and the received spectra of different schemes, respectively.

Fig. 5 illustrates the experimental BER versus received SNR for different schemes. At small compression factors, FTNmCAP-QGIM with k = 2 requires the lowest SNR compared with other schemes at a BER of  $3.8 \times 10^{-3}$ , while at larger compression factors, FTN-mCAP-VQGIM requires the lowest SNR and outperforms the other schemes. Take m = 6 as an example to illustrate. For  $\beta = 0.3$ , as shown in Fig. 5(a), to reach the 7% FEC coding limit, compared with 6CAP, FTN-6CAP and FTN-6CAP-GIM with k = 2, FTN-6CAP-GIM with k = 3 requires the smallest SNR of 9.0 dB. Compared with all schemes, FTN-6CAP-QGIM with k = 2 requires the smallest SNR of 5.3 dB, indicating an SNR gain of 3.7 dB compared with FTN-6CAP-GIM with k = 3. When the compression factor is increased to 0.35, Compared with all schemes, FTN-6CAP-VQGIM requires the smallest SNR of 9.8 dB. FTN-6CAP-QGIM with k = 2 and FTN-6CAP-VQGIM achieve the SNR gains of 2.8 and 3.8 dB in comparison to 6CAP, respectively.

#### IV. CONCLUSION

In this paper, we have proposed three spectral-efficient GIM schemes to address the non-negligible SE loss of GIM scheme for FTN-mCAP based bandlimited VLC systems. First, FTN-mCAP-QGIM is proposed to obtain a higher SE than FTN-mCAP-GIM, and an enhanced LLR detector is designed to reduce LLR detection errors. Second, FTN-mCAP-VGIM is proposed, allowing variable subband activation. Third, FTN-mCAP-VQGIM is proposed to further enhance the SE of FTN-mCAP-VGIM. The performance of three spectral-efficient GIM schemes has verified through simulations and experiments. Therefore, the proposed spectral-efficient GIM schemes hold significant potential for application in bandlimited VLC systems.

#### REFERENCES

- R. Struzak, T. Tjelta, and J. P. Borrego, "On radio-frequency spectrum management," *URSI Radio Science Bulletin*, vol. 2015, no. 354, pp. 11– 35, Sep. 2015.
- [2] N. Chi, Y. Zhou, Y. Wei, and F. Hu, "Visible light communication in 6G: advances, challenges, and prospects," *IEEE Vehicular Technology Magazine*, vol. 15, no. 4, pp. 93–102, Dec. 2020.
- [3] A. R. Ndjiongue, H. C. Ferreira, and T. M. N. Ngatched, "Visible light communications (VLC) technology," Wiley encyclopedia of electrical and electronics engineering, pp. 1–15, Jun. 1999.
- [4] D. H. Kwon, S. H. Yang, and S. K. Han, "Modulation bandwidth enhancement of white-LED-based visible light communications using electrical equalizations," in *Broadband Access Communication Tech*nologies IX, 2015, pp. 171–176.
- [5] C. Chen, Y. Nie, M. Liu, Y. Du, R. Liu, Z. Wei, H. Y. Fu, and B. Zhu., "Digital pre-equalization for OFDM-based VLC systems: centralized or distributed?" *IEEE Photonics Technology Letters*, vol. 33, no. 19, pp. 1081–1084, Aug. 2021.
- [6] H. Li, X. Chen, B. Huang, D. Tang, and H. Chen., "High bandwidth visible light communications based on a post-equalization circuit," *IEEE Photonics Technology Letters*, vol. 26, no. 2, pp. 119–122, Jan. 2014.
- [7] N. Chi, Y. Zhou, S. Liang, F. Wang, J. Li, and Y. Wang, "Enabling technologies for high-speed visible light communication employing CAP modulation," *Journal of Lightwave Technology*, vol. 36, no. 2, pp. 510– 518, Jan. 2018.
- [8] Y. Nie, C. Chen, S. Savovic, Z. Wang, R. Min, X. You, Z. Zeng, and G. Shen, "0.5-bit/s/Hz fine-grained adaptive OFDM modulation for bandlimited underwater VLC," *Optics Express*, vol. 32, no. 3, pp. 4537–4552, 2024.
- [9] M. I. Olmedo, T. Zuo, J. B. Jensen, Q. Zhong, X. Xu, S. Popov, and I. T. Monroy, "Multiband carrierless amplitude phase modulation for high capacity optical data links," *Journal of Lightwave Technology*, vol. 32, no. 4, pp. 798–804, Oct. 2014.
- [10] S. Liang, L. Qiao, X. Lu, and N. Chi, "Enhanced performance of a multiband super-Nyquist CAP16 VLC system employing a joint MIMO equalizer," *Optics Express*, vol. 26, no. 12, pp. 15718–15725, 2018.
- [11] J. Chen, Z. Wang, Y. Zhao, J. Zhang, Z. Li, C. Shen, and N. Chi, "Neural network detection for bandwidth-limited non-orthogonal multiband CAP UVLC system," *IEEE Photonics Journal*, vol. 14, no. 2, pp. 1–9, Apr. 2022.
- [12] W. Niu, Z. Xu, J. Shi, C. Shen, J. Zhang, and Z. Li, "Interference mitigation for faster-than-Nyquist multiband CAP visible light communication," *Journal of Lightwave Technology*, vol. 42, no. 13, pp. 4454– 4466, Jul. 2024.
- [13] Z. Wang, G. Li, F. Hu, and N. Chi, "Toeplitz concatenated matrix aided ICA algorithm for super-Nyquist multiband CAP VLC systems," *Optics Express*, vol. 28, no. 20, pp. 29876–29894, 2020.
- [14] Y. Nie, C. Chen, Z. Zeng, X. You, H. Haas, and G. Shen, "Interference mitigation for faster-than-Nyquist mCAP in bandlimited VLC: a lowcomplexity gapped index modulation approach," *Journal of Lightwave Technology*, vol. 43, no. 14, p. 6533–6546, Jul. 2025.